LASERLAB-EUROPE

The Integrated Initiative of European Laser Research Infrastructures III

Grant Agreement number: 284464

WP30 ï Laser and Photonics for Biology and Health (BIOPTICHAL)

Deliverable 30.7

Advanced microscopy techniques based on laser plasma X-ray sources

Lead Beneficiary: MUT-IOE

Due date: 31-05-2014 (M24)

Date of delivery: 31-05-2014 (M24)

Project webpage: www.laserlab-europe.eu

Deliverable Nature	
R = Report, P = Prototype, D = Demonstrator, O = Other	R
Dissemination Level	
PU = Public PP = Restricted to other programme participants (incl. the Commission Services) RE = Restricted to a group specified by the consortium (incl. the Commission Services) CO = Confidential, only for members of the consortium (incl. the Commission Services)	PU

A. Abstract / Executive Summary

In the report the development of a compact transmission soft X-ray microscope for biomedical applications is described. The microscope operates in the ñwater windowò spectral range and is based on a desk-top laser plasma X-ray source combined with an ellipsoidal grazing incidence mirror as a condenser for sample illumination, a hyperboloid/ellipsoid Wolter type I mirror as an imaging objective and a CCD camera to record an X-ray image. The laser plasma X-ray source is based on a gas puff target produced with nitrogen gas. The microscope allows to obtain magnified images of objects with sub-micron spatial resolution with the exposure time as low as a few seconds. The source and the microscope descriptions as well as the results of imaging for tests and biological objects are presented. The future plans regarding the development of the transmission soft X-ray microscope based on a diffraction Fresnel optics are discussed.

B. Deliverable Report

1 Introduction

Soft X-ray microscopes provide complementary information to the one obtained from optical and electron microscopy. Soft X-ray microscopy can deliver images of hydrated biological samples up to ~10μm thick, with nanometer spatial resolution. The soft X-ray microscopes operate in the ñwater windowô spectral range which spans between the carbon (4.3nm; 284eV) and oxygen (2.3nm; 540eV) *K* absorption edges. Within this spectral region, water is nearly an order of magnitude more transparent than organics. As a consequence, soft X-ray microscopes can image wet and intact biological specimens (without sectioning that is needed in case of electron microscopy). Additionally, soft X-ray microscopes can operate in atmospheric-pressure air as the penetration distance in atmospheric air is 0.4-4mm within the ñwater window", and for helium it is 20-100mm. The capability to image frozen-hydrated specimens has been developed to minimize image blurring associated with the thermal motion. Detailed information on soft X-ray optics and microscopy one can find in the references [1-4].

The transmission soft X-ray microscopes (SXRM) currently in operation rely on high brightness synchrotron radiation sources in order to achieve short exposure times. Theses microscopes are based on diffraction Fresnel optics which use zone plates as objective lenses for high resolution imaging. The SXRM of this type was first developed at the University of Goettingen in Germany [5] and at the SUNY at Stony Brook (USA) [3]. Since then, several soft X-ray microscopes have been developed and installed at various synchrotrons around the world and their applications in biomedical research have been demonstrated in numerous publications. However, because of some reasons, synchrotron based SXRM is not very convenient for the users as compared with traditional laboratory microscopes. Therefore, compact non-synchrotron soft X-ray microscopy has been developed, gaining more interest. Such microscopes employ compact laser plasma or discharge plasma sources. Several systems have been developed at various laboratories. They are mostly based on laser plasma sources with solid or liquid targets and Fresnel optics. Examples of such systems are described in the references [6-12].

In this report we present a compact transmission soft X-ray microscope based on a desk-top laser plasma X-ray source. An ellipsoidal grazing incidence mirror is used as a condenser for sample illumination, a hyperboloid/ellipsoid Wolter type I mirror is acting as an objective and a CCD camera is used for registration of magnified X-ray images. The laser plasma X-ray source is based on an argon gas puff target and irradiated with nanosecond high-intensity ($\sim 10^{12} Wcm^{-2}$) laser pulses form a commercial Nd:YAG laser. Microscopic images of test objects and biological dry samples have been registered with sub-micron spatial resolution at the exposure time as low as a few seconds. The development of the soft X-ray microscope with the Wolter type I mirror as an objective is the first step in the development of the transmission soft X-ray microscope based on a diffraction Fresnel optics. Schematic of a new microscope and its brief description is presented.

2 Objectives

The main objective of this work is the development of advanced microscopy techniques exploiting pulsed laser sources to extend spectral excitation range, penetration depth, sensitivity, and selectivity, temporal and spatial resolution (Objective OBJ2). It has been done by the development of a desk-top soft X-ray microscope based on a compact laser plasma source (Task 2.B.6). The detailed objectives of this research are:

- demonstration of the transmission soft X-ray microscope with grazing incidence Wolter type optics,
- demonstration of the transmission soft X-ray microscope with Fresnel optics.

The last objective will be achieved at the end of the project realization.

3 Work performed / results / description

The optical scheme of the transmission soft X-ray microscope based on grazing incidence reflective optics is shown in Fig. 1. The microscope is equipped with an ellipsoidal grazing incidence mirror coated with nickel as a condenser to focus soft X-ray radiation onto an object. A hyperboloid/ellipsoid Wolter type I mirror was used as an objective to form a magnified image onto a soft X-ray sensitive CCD camera in transmission mode. The experimental arrangement of the ellipsoidal condenser and the objective are shown in Fig. 2. The use of the gas puff target to create laser plasma emitting soft X-ray radiation eliminates debris production problem associated with solid targets. Radiation in the "water-window" spectral range was selected by a titanium filter. Test objects" two distinct patterns of copper meshes were imaged with a half-pitch spatial resolution approaching 1 μm in a very compact set up and with short exposures.

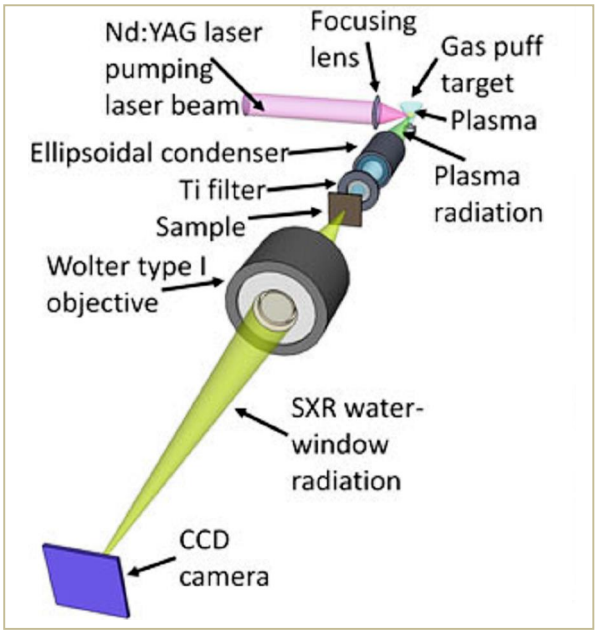

Fig. 1. Optical scheme of the transmission soft X-ray microscopy system based on grazing incidence reflective optics.

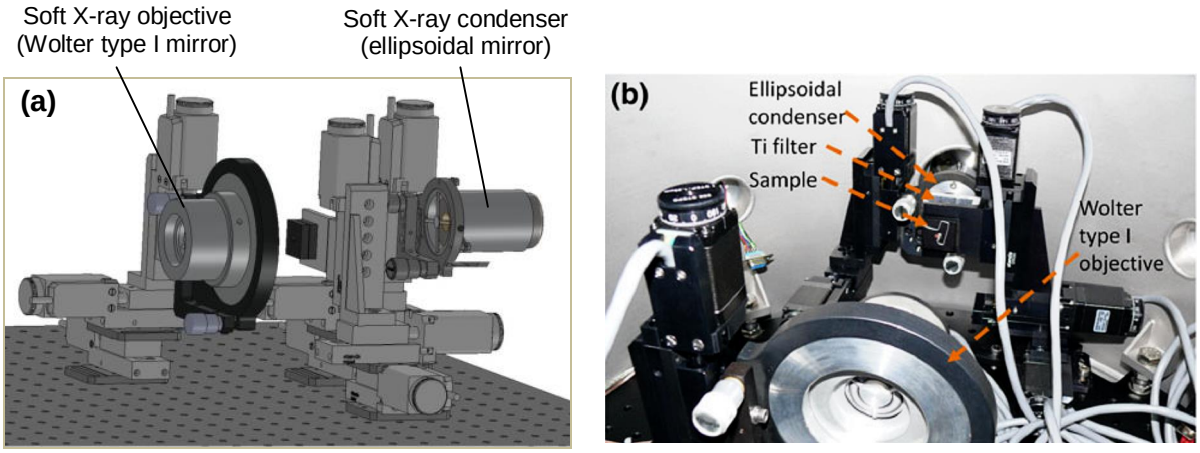

Fig. 2. The experimental arrangement of the ellipsoidal condenser and the objective.

The laser plasma source, used in the experiment, has been developed for EUV metrology applications in the frame of MEDEA+ project [13] and was, after modification for efficient emission of soft X-ray radiation, including the "water-window" spectral region, previously reported in [14]. This source has the advantage over other compact sources that it is a debris free source and has a possibility to change working gases, thus allowing to change both the peak emission wavelength and the inverse relative bandwidth of the emission.

In the soft X-ray microscope Ar plasma was produced by focusing of the pumping laser pulses, from Nd:YAG laser (Ekspla), with duration of 4 ns and energy of 0.74 J by an f = 25 mm focal length lens onto a gas puff target. The plasma radiates in a very broad range of wavelengths, including soft X-ray region and by using additional spectral filtering it is possible to tailor the spectral emission of the source. The source can operate up to 10 Hz repetition rate. A pressure of 1.5×10^{-4} mbar was constantly maintained in the microscope chamber during the source operation. The experimental setup is extremely compact. The microscope is located inside a vacuum chamber, 60 cm in diameter and 35 cm in height and the entire system fits on top of a single 1.8×1.2 m^2 optical table. Schematic of the microscope is presented in Fig. 3. Fig.4 shows the experimental arrangement of the microscope setup. The microscope installed in the laboratory is shown in Fig. 5.

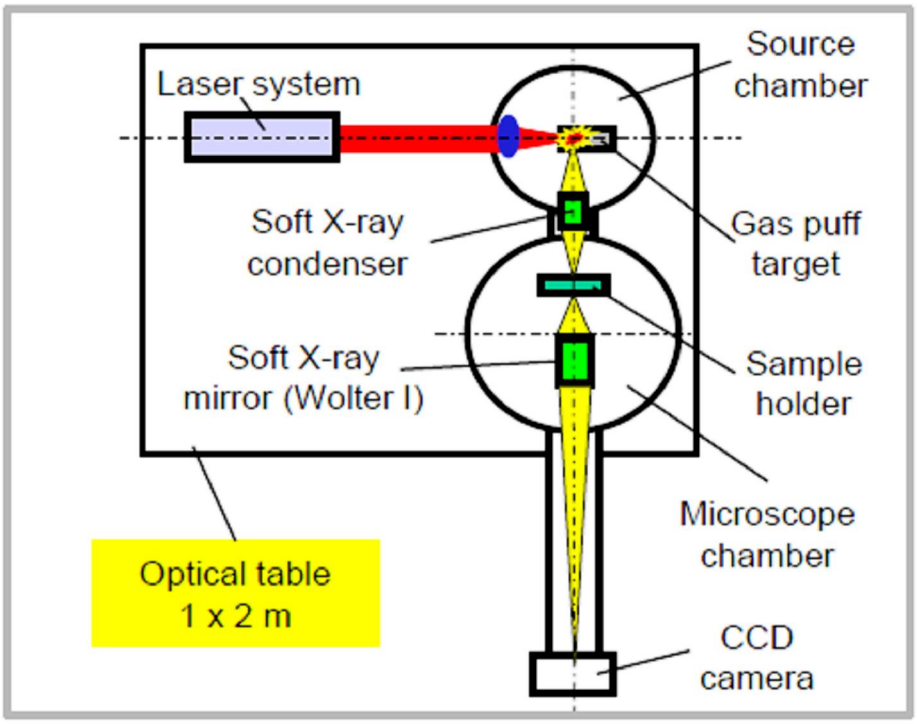

Fig. 3. Schematic of the transmission soft X-ray microscope based on grazing incidence reflective optics.

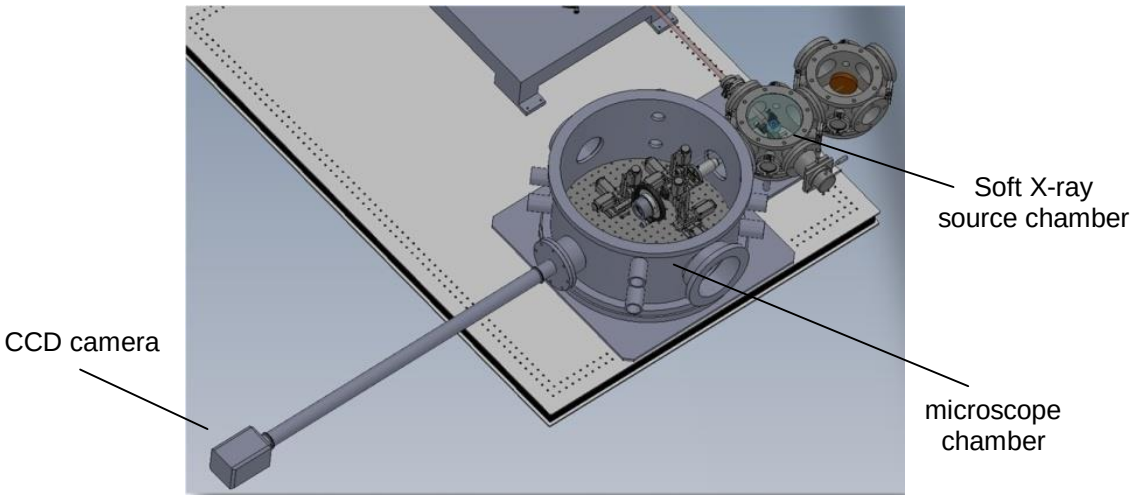

Fig. 4. The experimental arrangement of the microscope setup.

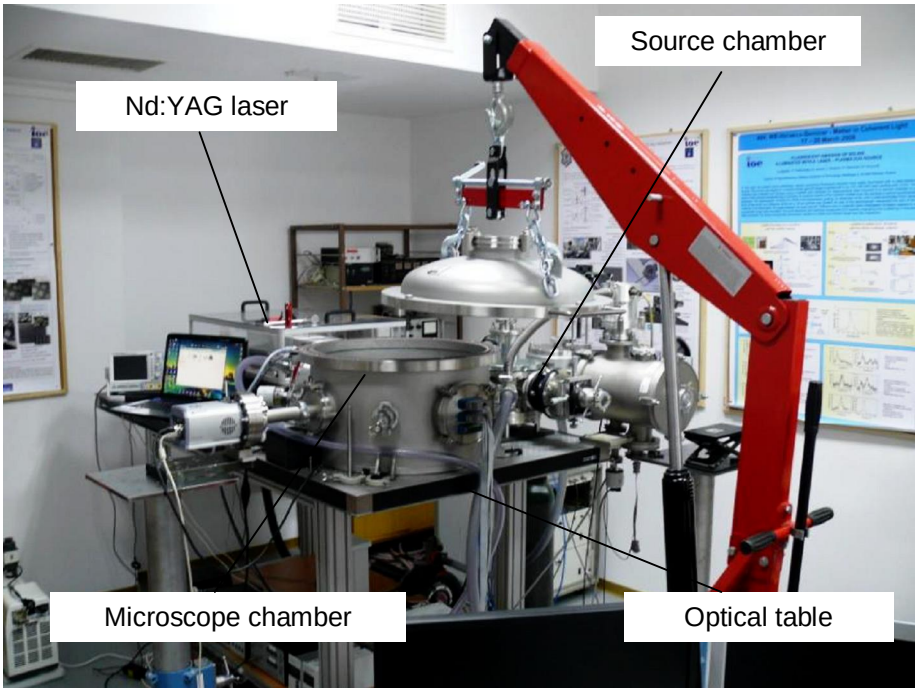

Fig. 5. Transmission soft X-ray microscope based on grazing incidence reflective optics.

Soft X-ray radiation from the plasma was collected and focused by an ellipsoidal, axi-symmetrical nickel coated condenser mirror (Rigaku, Inc.) The condenser is a broad-band optic, capable of efficiently reflecting radiation from the EUV range down to soft X-ray region with energy cut-off of about 600 eV (~2.06 nm critical wavelength). The distance between foci of the condenser was equal to 270 mm. The distance from the plasma, positioned in the first focal plane, to an entrance plane of the condenser was 140 mm, while the distance from an exit plane to the second focal planeð 60 mm. Entrance diameter was equal to 14 mm and results in entrance numerical aperture of NA_{C_in} = 0.05, while the exit diameter of 11.7 mm corresponds to exit numerical aperture ofN_{AC_out} = 0.09.

The laser plasma source was optimized for efficient generation of SXR radiation from argon plasma. The target is formed by two circularly symmetric nozzles. The inner nozzle, 0.4 mm in diameter, injects a small amount of working gas (argon) into the vacuum, 250 μs after arrival of synchronization pulse from laser power supply. The nozzle stays open for 600 μs. The outer nozzle, ring-shaped 0.7ï 1.5 mm in diameter, injects a small Z-number gas, in our case helium, to narrow down the flow of the working gas, reducing its density gradient along the normal to the nozzle axis. The nozzle opens 750 μs after arrival of the synchronization pulse and stays open for 200 μs. A 50 μs later the laser pulse is generated producing in turn a soft X-ray pulse. The nozzle axis was positioned almost concentrically with the laser focal point, displaced 0.1 mm in the direction opposite to the condenser optic, to reduce the reabsorption of soft X-ray radiation in a neutral gas from the target. The distance from the focal point to the nozzle plane was 1.5 mm to avoid nozzle damage by plasma formation.

To spectrally narrow the emission from argon plasma a 200 nm thick, 10 mm in diameter, free-standing titanium filter (Lebow) was used, positioned 21 mm downstream the condenser. Spectrally filtered radiation illuminates the sample, positioned 60 mm downstream the condenser, inits second focal point. Then, the sample is imaged onto a soft X-ray- sensitive back-illuminated, 1,024 × 1,024 pixels, 13 × 13 μm^2 pixel size, CCD camera (Andor) by a Wolter type I reflective objective. The objective is composed of two axially symmetric ellipsoidal and hyperboloidal nickel coated mirrors. The object plane of the objective, which coincides with the sample plane, is located ~150 mm from its entrance aperture, 15 mm in diameter with 14 mm central beam stop. The image plane is ~2,190 mm

from the objectiveôs exit aperture, 17 mm in diameter with 15.5 mm diameter central beam stop. The magnification of the objective is thus equal to 14.6× and the image pixel size is 890×890 nm^2. The entrance numerical aperture of the objective is equal to NA_{O_in} = 0.05, while the exit numerical aperturedð NA_{O_out} = 0.0038. Exit numerical aperture of the condenser (NA_{C_out} = 0.09) is almost twice the objective entrance NA_{O_in}, providing incoherent illumination [15], since $\sigma = NA_{C\ out}/NA_{O\ in}$ = 1.8.

The condenser, sample stage and objective were mounted on three axis translation stages driven by vacuum compatible step motor actuators (Standa). To obtain a single image in the ówater-windowô spectral range 50ï 100 pulses were necessary, at 10 Hz repetition rate. During image acquisition the CCD camera was cooled down to -10 °C to decrease the intrinsic, thermal noise of the detector.

Measurements of the source photon flux were performed using commercial AXUV100 silicon pï n junction photodiode (IRD, Inc.) and corrected for transmission of the Ti filter. Measured number of photons was equal to 1.3 × 10^{11} photons/sr/pulse or 1.6 × 10^{12} photons in a 4π solid angle per soft X-ray pulse, in the transmission band of the filter (from 2.8 to ~6 nm wavelength), assuming a uniform angular distribution of emitted photons. Subsequent measurements yielded the number of photons in the focal plane of the condenser, equal to 3.6 × 10^{10} photons/pulse, which corresponds to 2.3 μJ/pulse in band.

The soft X-ray spectra, obtained with and without the filter have been measured using a transmission grating spectrometer equipped with 5,000-lines/mm free-standing grating, 33 μm entrance slit and a CCD camera (Andor). The grating was positioned ~680 mm from the plasma, the entrance slit was placed 4 mm from the grating and distance between the grating and the CCD was 145 mm. From geometry of the spectrometer and the grating, the wavelength range was up to 16 nm. The inverse relative bandwidth (IRB) of the spectrometer was estimated from the spectrum to be $\lambda/\Delta\lambda \sim 50$ at 4 nm wavelength. The spectrum of Ar plasma, both direct and filtered by Ti filter is shown in Fig. 6a. The spectrum obtained without the filter required only 5 pulses, while the one obtained with the filter required 100 soft X-ray pulses. Figure 6b, c shows raw data from the CCD camera for both spectra.

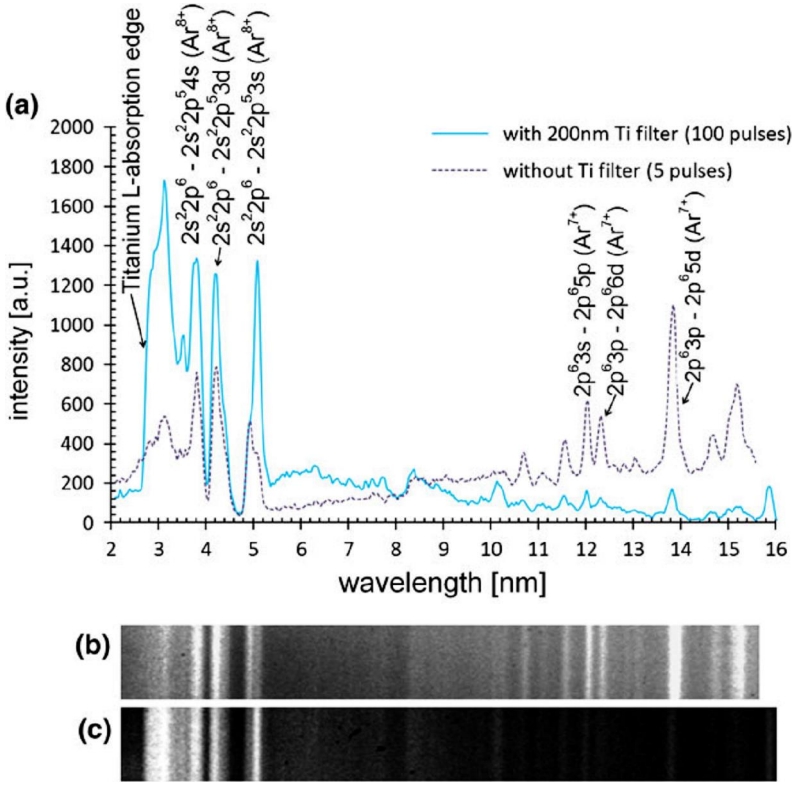

Fig. 6. Spectrum of the soft X-ray radiation (a) and CCD data without (b) and with (c) Ti 200 nm filter, respectively.

The figure depicts Ar emission spectrum in the wavelength range from 2 to 16 nm. The dominant groups of argon spectral lines are Ar^{8+}: $2s^2\ 2p^6$-$2s^2 2p^5 4s$, wavelengths between λ = 36.78 Å and λ = 36.96 Å , Ar^{8+}: $2s^2\ 2p^6$-$2s^2 2p^5 3d$ (λ = 41.48ï 42.56 Å), Ar^{8+}: $2s^2 2p^6$-$2s^2 2p^5 3s$ (λ = 48.73ï 49.18 Å). In the longer wavelength range, filtered out by Ti filter, the dominant spectral groups are: Ar^{7+}: $2p^6 3s$-$2p^6 5p$ (λ =120.09ï 120.16 Å), Ar^{7+}: $2p^6 3p$-$2p^6 6d$ (λ = 122.62ï 123.03 Å) and Ar^{7+}: $2p^6 3p$-$2p^6 5d$ (λ = 137.93ï 138.44 Å), according to the data reported in [16]. Most of the spectrally filtered radiation is from the ówater-windowö spectral range, usually defined as the wavelength range from 2.3 to 4.4 nm.

A spatial distribution of the Ar plasma in the ówater-windowö spectral range was obtained using a pinhole camera. The measurements were performed with Ti filter, to assess the plasma size particularly in the ówater-windowö range. Laser drilled, 32 μm in diameter pinhole was positioned 291 mm from the plasma and 280 mm from the CCD camera (Reflex), which was equipped with 512 × 512 pixels CCD chip, 0.5 × 0.5 in^2 in size. This results in a lateral magnification of 0.96×. The spatial distribution of the Ar plasma in the ówater-windowö spectral range is depicted in Fig. 7a and cross sections in vertical and horizontal directions are shown in Fig. 7b. For the measurements 300 pulses were required. The argon plasma FWHM size was measured to be 240×130 μm^2.

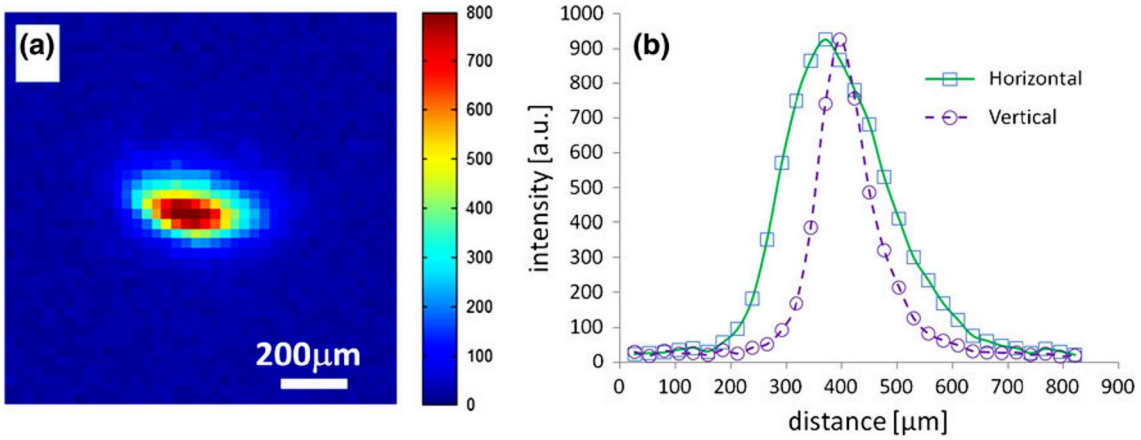

Fig. 7. Pinhole camera image of plasma spatial intensity distribution (a) and cross-sections in horizontal and vertical directions (b).

To illuminate the sample uniformly a proper condenser alignment was necessary. For that a small beam block, ~5 mm in diameter, was placed at the exit plane of the condenser, to block a direct light from the plasma. Radiation, focused by the condenser, was then scattered by a 750 nm thick Al film placed in the vicinity of the focal plane of the condenser. Scattered light was imaged on to a CCD camera (Andor) by previously mentioned pinhole camera, to form a slightly magnified image of the spatial distribution of light downstream the condenser near its focal plane. The distance from the Al foil to the pinhole was equal to 360 mm and from the pinhole to the detectorð 325 mm, resulting in lateral magnification of 1.11×. The optimization of the condenser position was performed and the examples of intensity distributions of scattered radiation from the Al foil, focused by the condenser optic, for different condenser position are shown in Fig. 8. If the condenser is properly aligned, the intensity distribution is circularly symmetric and has smallest area, as shown in Fig. 8b. However, if the optic is misaligned the images of the focal plane show asymmetry and the spot is bigger, yielding lower photon density at the focal plane, Fig. 8a, c. The numbers, shown for each figure, correspond to a distance of the condenser from its optimal position. In this example, the condenser was misaligned in the plane perpendicular to the optical axis of the system.

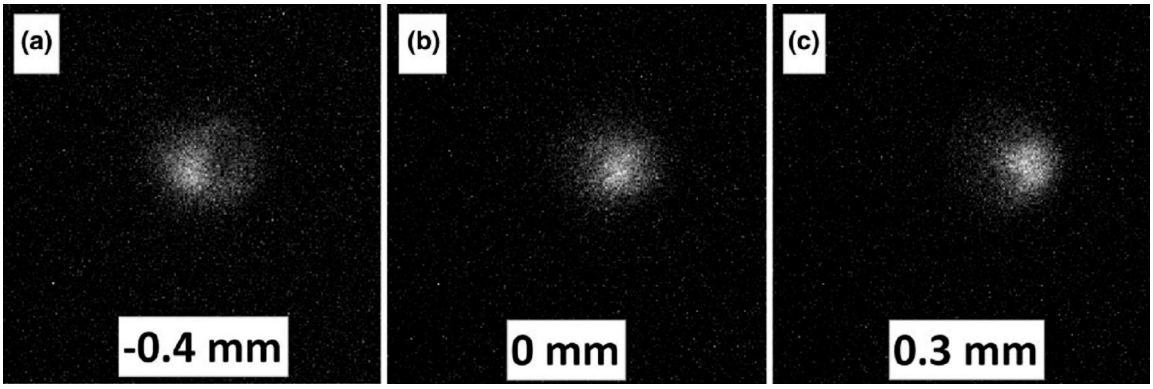

Fig. 8. Intensity distribution of the radiation, obtained by scattering of soft X-ray radiation from 750 nm thick Al foil, focused by an ellipsoidal condenser if properly aligned (b) and for slightly misaligned condenser in direction perpendicular to the optical axis, around the optimal position (a, c). Numbers indicate the amount of misalignment (distance).

As test objects, two transmission electron microscope (TEM) grids (meshes) (Tesla) of different geometries were used. Typical scanning electron microscope (SEM) images of the objects are shown in Fig.9. A square-shaped mesh, shown in Fig. 9a, has a period of (123.8 ± 0.5) μm and a bar with width (42.9 ± 0.7) μm, while a rectangular mesh, shown in Fig. 9b, has a period of (83.2 ± 1.4) μm and a slit width of (37.1 ± 0.8) μm. The errors are associated with the accuracy of grating fabrication. The thickness of both grids was ~13 μm. Dashed boxes indicate the regions of the sample imaged with the "water-window" microscope.

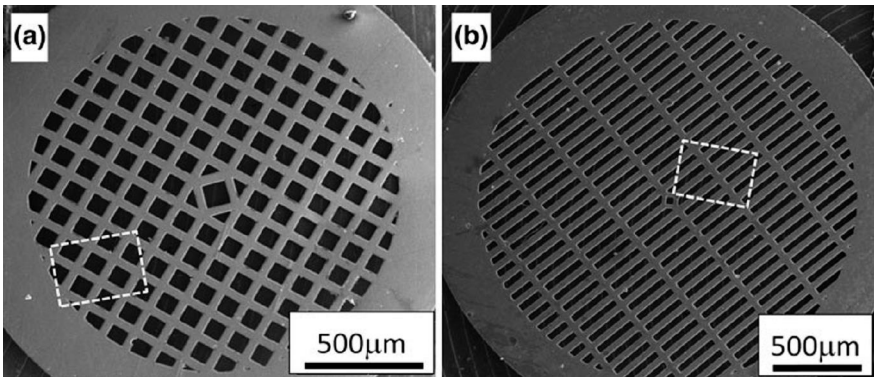

Fig. 9. SEM images of the test objects: square mesh (a) and rectangular mesh (b).

To obtain the sharpest possible image in the "water-window" spectral range, series of images were recorded at various sample-objective distances, in the range of ±2 mm from the focal point of the objective. From the entire set of images, the "sharpest" image was chosen for subsequent resolution measurements. Resolution of the microscope was assessed by a well established knife edge (KE) test. For incoherent illumination the 10÷90 % intensity transition across a sharp edge corresponds to a well known Rayleigh resolution and to twice the value of half-pitch grating resolution of the optical system [4].

Typical images of the meshes, obtained under argon plasma illumination, filtered by 200 nm thick Ti filter are shown in Fig. 10a, for square mesh and b for a rectangular mesh, respectively. Black dotted line, depicted in Fig. 10a, indicate the region, where subsequent KE resolution measurements were carried out. A typical KE lineout is depicted in Fig. 11, where 10÷90 % intensity transition in the normalized lineout through the sharp edge in the image is equal to ~2.5 pixels. For the pixel width of 890 nm, it yields 2.2 μm Rayleigh resolution. The value of resolution was assessed statistically, based on 10 independent measurements, resulting in half-pitch spatial resolution equal to r_{KE} = 1.1 ± 0.2 μm.

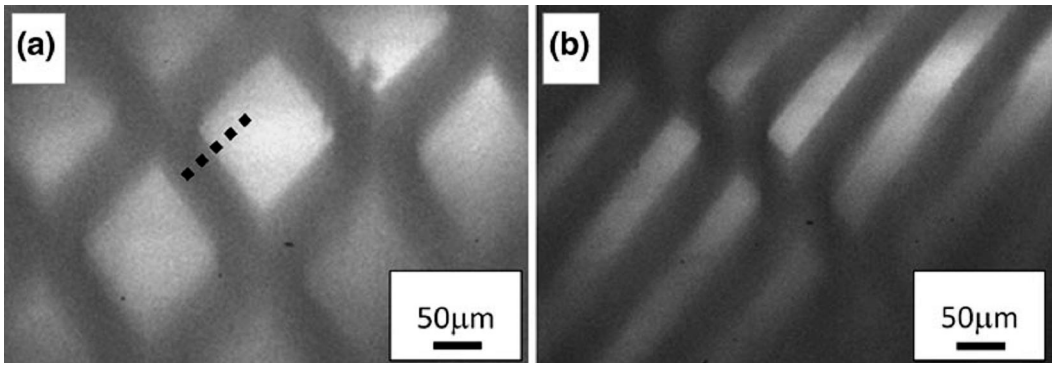

Fig. 10. Soft X-ray microscopy images of the test objects (a, b), shown in Fig. 9, obtained in the "water-window" spectral region. Dotted line indicates region where a lineout was made to assess spatial resolution based on the KE test

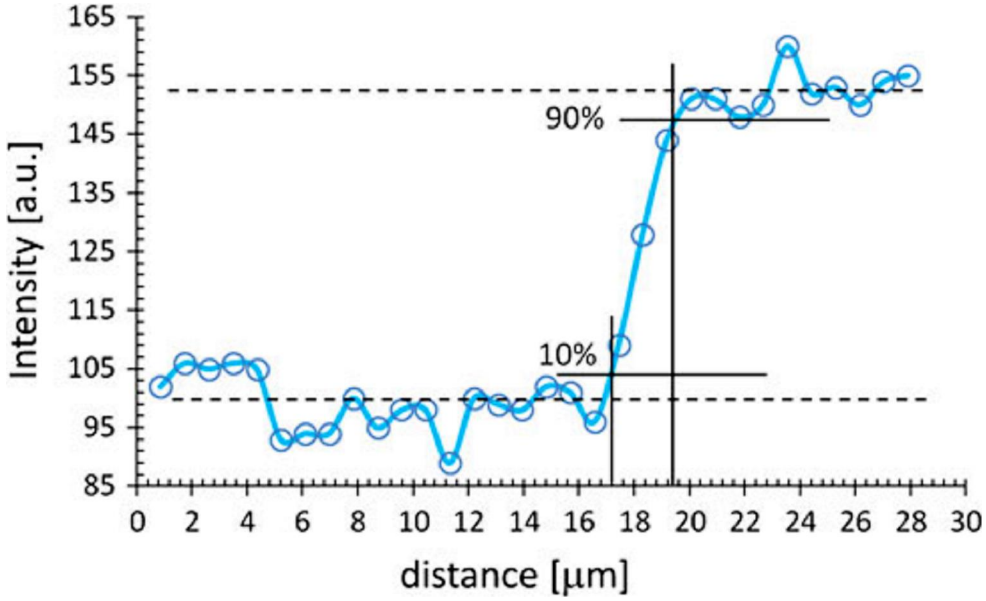

Fig. 11. KE resolution test result showing Rayleigh resolution equal to 2.5 pixels = 2.2 µm or half-pitch spatial resolution equal to 1.1 µm.

The theoretical half-pitch resolution of the microscope can be expressed as $r_{KE} = k\lambda/(2NA_{O\,in})$, where k is illumination and resolution test specific dependent constant, for incoherent illumination (k = 0.61) this resolution is equal to 18.3 nm at assumed λ = 3 nm (peak transmission of the Ti filter, just near the absorption edge), so it is much better than measured half-pitch resolution of 0.9 µm in the best case (statistically mean value is 1.1 µm). However, the Wolter objective is not a full aperture optic, in fact has a central beam block forming a thin, annular shaped entrance aperture, with outer radius r_o = 7.5 mm and inner radius r_i = 7 mm, with obscuration ratio c equal to $c = r_i/r_o = 0.93$. This leads to a different shape of a point spread function (PSF), which even though has a smaller central lobe, as can be seen in Fig. 12a, but it still has much more pronounced secondary lobes, which extend to a few hundreds of nm from the center, carrying out much more energy than comparing to a little wider PSF function for a full, un-obscured entrance aperture of hypothetical objective. Figure 12b shows corresponding knife edge functions (KEF) for previously described two types of apertures, calculated based on their PSF functions. A half-pitch spatial resolution

for un-obscured aperture, which in our case will be a theoretical resolution limit, is equal to ~18.5 nm. For annular entrance aperture, with c = 0.93, the expected half-pitch resolution is much worse, equal to 304 nm, which is more than 16× the diffraction limit. Blue solid line with data points shows the experimentally obtained KEF, from which the half-pitch resolution of 1.1 μm was obtained, with lower, l.b. (900 nm) and upper u.b. (1.3 μm) bound on the resolution from statistical measurements; gray and black solid lines, respectively.

Second parasitic parameter that influences the spatial resolution, which was previously studied in EUV microscopy [17, 18], is a thickness of the object. Owing to the fact that sometimes the thickness of the object is much larger than the depth of focus (DOF), it causes the resolution to be much worse, that for the case of óthinô object. The DOF, defined usually for 20 % intensity decrease, can be calculated for a full aperture objective using DOF = ± λ/(2NA$^2_{Oin}$ and assuming λ = 3 nm, is equal to ±600 nm, or 1.2 μm in total, for 50 % intensity drop, however, it was calculated to be 2.09 μm. For objective, with obscuration ratio c = 0.93, and 50 % intensity drop, the DOF is much larger and equal to 30.15 μm. Thus, due to the fact that the thickness of the test objects, d = 13 μm, is much smaller than the DOF, so its influence on spatial resolution was assumed to be negligible.

Another resolution decreasing factor is the influence of modulation transfer function (MTF) of the CCD detector with relatively large equivalent pixel size of 890 × 890 nm^2 in compared to measured spatial resolution. PSF of the CCD detector in this case will additionally widen computed PSF and KEF for the optical system. Convolution of these two parameters yields the expected half-pitch resolution to be equal to ~480 nm and corresponding KE function (KEF) can be seen in Fig. 12b as a solid violet line.

Additional discrepancy is probably due to optical quality of the Wolter objective mirrors, surface curvature errors, resulting in various aberrations and finally surface roughness of the two-mirror Wolter objective optical system. Particularly, the later might have a noticeable contribution for large r/λ (r ï rms roughness of the mirror), especially for such a short wavelength λ= 3 nm, where only a fraction of the total energy resides in the specular beam, described by functions obtained from diffraction calculations and presented in Fig. 12a, while the remaining energy is contained in scattered components [19]. More detailed calculations of the contribution of this effect are under way.

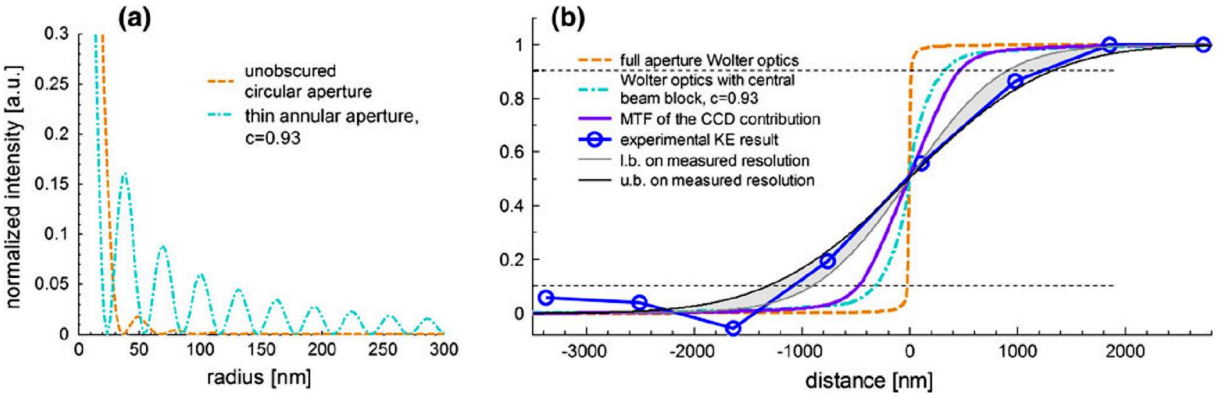

Fig. 12. Calculated PSF functions (a) and KE functions (b) for un-obscured, full aperture hypothetical objective (dashed line), objective with central beam block (thin annular entrance aperture), for c = 0.93 (dash-dotted line), such as Wolter type I objective used in the experiment. In addition in (b) MTF contribution of the CCD detector ð violet solid line, KE function obtained experimentally (solid line with circular markers) and statistically measured u.b. and l.b. on KE resolution (indicated with grey area).

The quality of microscope images strongly depends on the exposition time. Examples of the images of the test object registered for various exposition times are presented in Fig. 13. Possibility of a single-shot exposure registration of a soft X-ray microscopy image was demonstrated.

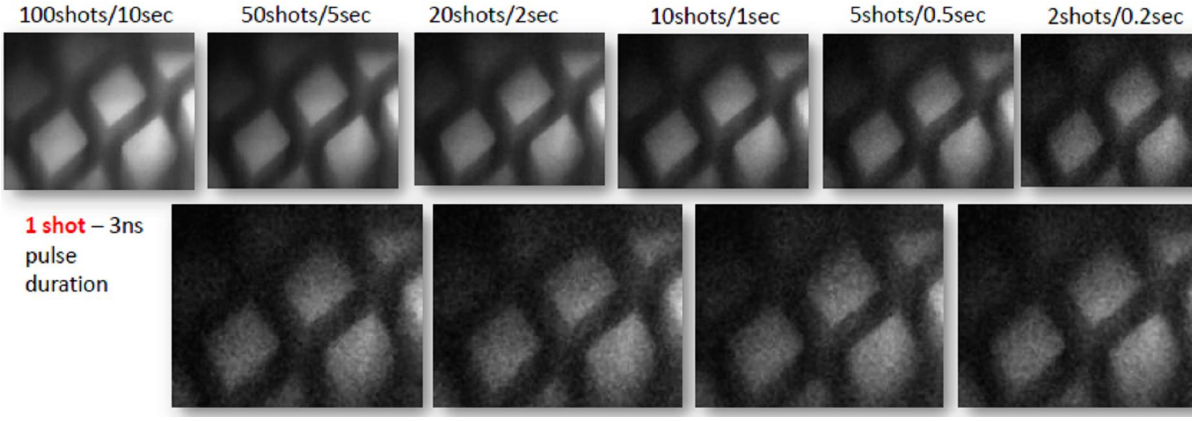

Fig. 13. Soft X-ray microscopy images of the test object registered for various exposure times.

The microscope was also used in the preliminary test for imaging of biological samples. As an object an onion skin was applied. The optical microscope image of onion skin cells is presented in Fig. 14a. The first soft X-ray microscopy images in the ówater-windowö spectral range of the onion skin cells, obtained using our system, are shown in Fig. 14b.

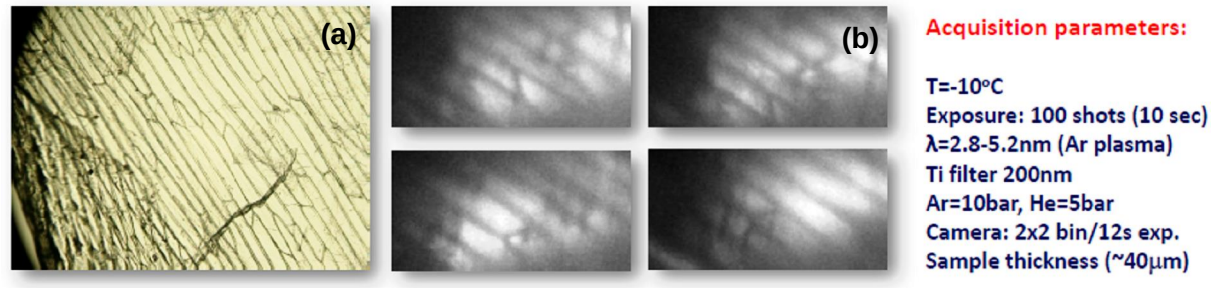

Fig. 14. Optical microscopy image of onion skin cells (a) and soft X-ray microscopy images (b).

4 Conclusions

We reported on ówater-windowö compact, desktop soft X-ray microscopy system, employing a laser-plasma source based on a double-stream gas-puff target and a Wolter type I objective. This system allows capturing magnified images of the objects, with magnification of ~15×, ~1 μm half-pitch spatial resolution and exposure time as low as 5s. The detailed characterization and optimization studies of the source and the microscope setup were described and discussed. The results presented in this report have been published in the scientific article [20].

Spatial resolution of this system is still quite unsatisfactory for many applications. The system, however, offers imaging capability in the ówater-windowö spectral range, combining its desktop size, accessibility and simple operation. The lack of dispersion of the condenser and objective and the possibility to change spectral emission of the source by changing the working gas or just the filters allows to perform imaging in other wavelength ranges, for example 18ï 60 nm using Al filter. This opens new possibilities to exploit different spectral information, now possible to obtain from investigated objects at various wavelengths using a single system and allow in turn to study the samples more thoroughly.

Future plans include improvement of the magnification and the spatial resolution of this system by changing the objective to a Fresnel zone plate (ZP), which offers spectral selectivity as well as much higher magnifications and spatial resolution, however, for the price of higher exposures. We also plan to change from argon to nitrogen plasma, where the emission is quasi-monochromaticð much more suitable for high dispersion ZP objectives.

5 References/Publications

1. A.G. Michette, *Optical systems for soft X-ray rays*, Plenum Press 1986
2. A.G. Michette, Rep. Prog. Phys. **51** (1988) 1525
3. J. Kirz, C. Jacobsen, M. Howels, Q. Rev. Biophys. 28 (1995) 33
4. D. Attwod, *Soft X-rays and extreme ultraviolet radiation: principles and applications*, Cambridge University Press, 1999
5. G. Schmal *et al*., Optik **93** (1993) 95
6. L.B. Da Silva *et a*l., Science **258** (1992) 269
7. S. Nakayama *et al*., Jap. J. Appl. Phys. **33** (1994) 1280
8. M. Berglind *et al*., J. Microsc. **197** (2000) 268
9. G.A. Johansonn *et al*., Rev. Sci. Instr. **73** (2002) 1193
10. M. Kishimoto *et al*., J. Phys. IV **104** (2003) 141
11. M. Wieland *et al*., Ultramicroscopy **102** (2005) 93
12. K.W. Kim *et al*., Phys. Med. Biol. **51** (2006) N99
13. H. Fiedorowicz *et al*., J. Alloys & Compd. **401** (2005) 99
14. P.W. Wachulak *et al*., Nucl. Instr. Meth. B **268** (2010) 1692
15. J.M. Heck *et al*., J. X-ray Sci. Technol. **8** (1998) 95
16. R.L. Kelly, J. Phys. Chem. Ref. Data **16** (1987) 386
17. P.W. Wachulak *et al.,* Opt. Lett. **35** (2010) 2337
18. P.W. Wachulak *et al*., Opt. Express **19** (2011) 9541
19. J. Harvey *et al*., Opt. Eng. **49** (2010) 063202
20. P.W. Wachulak *et al.,* Appl. Phys. B **111** (2013) 239, DOI 10.1007/s00340-012-5324-y